Journal of Materials Chemistry A

Accepted Manuscript

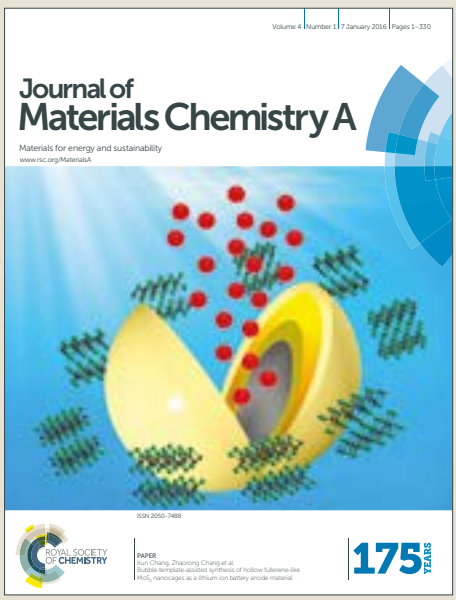

ROYAL SOCIETY OF CHEMISTRY

rsc.li/materials-a

View Article Online
DOI: 10.1039/C8TA12190G

Journal Name

ARTICLE

Selective host-guest interactions in metal-organic frameworks via multiple hydrogen bond donor-acceptor recognition sites

Received 00th January 20xx,
Accepted 00th January 20xx

DOI: 10.1039/x0xx00000x

www.rsc.org/

T. Wittmann,[a] C. B. L. Tschense,[a] L. Zappe,[a] C. Koschnick,[b] R. Siegel,[a] R. Stäglich,[a] B. V. Lotsch,[b] J. Senker*[a]

Targeted recognition of medium sized molecules with mixed hydrogen bond units is essential for using porous materials for molecular separation, sensing and drug delivery. One promising way to achieve selectivity, is to make use of the key-and-lock principle guiding the design of hydrogen bond receptors matching the chemical signature of the target molecules. Among the class of porous materials metal-organic frameworks are particularly well suited for this purpose, as they allow for functionalizing the inner surfaces with various pending groups. Here we report the successful incorporation of 2-pyridyl urea (URPy) side groups with hydrogen bond donor-donor-acceptor (DDA) patterns into the framework MIL-101 with pores in the mesoporous range. Their influence on the sorption properties was investigated by competitive adsorption of 2-aminopyridine (2-AP) and 3-aminopyridine (3-AP) on MIL-101-URPy (Al, Cr) derivatives and comparison to the behaviour of a single donor function within MIL-101-NH_2 (Al, Cr) derivatives. Grafting the coordinatively unsaturated sites at the inorganic building units (IBUs) with diethylamine, additionally allowed the adsorption at these sites to be suppressed and thus to focus on the hydrogen bond receptors. Compared to the single D sites the selectivity of 2-AP over 3-AP is enhanced by a factor of five for the DDA pending groups. Based on ^{15}N NMR spectroscopy and DFT calculations this observation is explained by forming double hydrogen bonds between the pyridyl urea groups and the 2-AP molecules, while 3-AP exhibits a single hydrogen bond only. At the D site of MIL-101-NH_2 both 2-AP and 3-AP form single hydrogen bonds only.

Introduction

Porous materials have potential for purification of gasses[1–3] and liquids,[4,5] drug delivery[6–8] and sensing.[9,10] The desired selectivity for host-guest interactions might be achieved by matching size, shape and binding preferences of guest molecules with the framework topology, respectively.[11–13] For example, kinetic separation with respect to size and shape is exploited for molecular sieving with zeolites, which requires rigid and periodic structures with uniform pores and windows.[1] Thermodynamic separation based on preferred binding sites, is achieved by providing chemical functionalities adapted in type and strength to targeted guest molecules. This includes van-der-Waals interactions, single and multiple hydrogen bond pattern, π–π-interactions and reversible bond formation for Lewis acid/base pairs.[1–3] This type of selectivity is widely spread for metal-organic frameworks (MOFs) due to their modular constitution and hybrid character. In particular, the organic linkers can be functionalized in many different ways by direct synthesis and postsynthetic modification (PSM), respectively.[14–18]

For example, subtle differences within the van der Waals interactions by introducing polar framework sites were exploited to increase the affinity for adsorbing carbon dioxide preferentially over nitrogen and methane.[2] Single hydrogen bonds accounted for the enhanced binding strength towards acetone compared to ethanol and water in MIL-53(Al)-NHCHO.[19] The selectivity for *ortho*-xylene over the *meta* and *para* analogues for MIL-53 (Al, Fe)[20,21] was explained by a simultaneous interaction of the two methyl units with two carboxylate groups of the terephthalate linkers, which is possible only for o-xylene due to the four-sided channel-type pores.[20] In contrast, the pronounced selectivity for p-xylene in MIL-47(V), MIL-125(Ti), MIL-125(Ti)-NH_2 and CAU-1(Al) solely arises from the shape of their cavities promoting a more efficient molecular π-π stacking of the respective isomer.[22,23]

Coordinatively unsaturated metal sites (CUS) lead to even higher sorption affinities and selectivities by adjusting coordination bonds via the Lewis acidity of the metal ions. For instance, CUSs with hard Lewis acidic metals as in MIL-100 (Al, Fe, Cr, V)[24] and MIL-101 (Cr)[20–23] proved to be effective for adsorption of hard Lewis basic N-heterocyclic compounds, whereas CUSs with softer Lewis acidic metals like HKUST (Cu)[29] and CPO-27 (Ni, Co)[25,30] preferred softer Lewis basic sulphur compounds.

However, controlled loading and release of more complex molecules bearing several functional groups like substituted heterocycles cannot be realized by molecular sieving and unspecific functional groups (e.g. -NH_2, -OH); it requires specific interactions. These might be achieved by supramolecular binding motifs, which are common for the formation of biological and artificial self-assembly systems.[31–

[a] University of Bayreuth, Inorganic Chemistry III and Northern Bavarian NMR Centre (NBNC), Universitätsstraße 30, 95440 Bayreuth, Germany. E-mail: juergen.senker@uni-bayreuth.de
[b] Max Planck Institute for Solid State Research, Heisenbergstr. 1, 70569 Stuttgart, Germany and Department of Chemistry, University of Munich (LMU), Butenandtstr. 5-13, 81377 Munich, Germany Address here.
† Footnotes relating to the title and/or authors should appear here.
Electronic Supplementary Information (ESI) available: [details of any supplementary information available should be included here]. See DOI: 10.1039/x0xx00000x

[34] They strongly rely on non-covalent π–π-interactions and multiple hydrogen bond networks[35] where geometric and electrostatic complementarity between host and guest drives their association.[36] This opens up the design of host-guest adducts that respond to certain external physical and chemical stimuli.[32,36,37] The reversibility of such binding patterns mainly depends on the strength of the multiple H-bond pattern and competing solvent-guest interactions. The former can be controlled by size and sequence of donor-acceptor units providing favorable or unfavorable binding sites.[35,38]

Although, the incorporation of supramolecular building blocks into MOFs has been shown in several studies,[39] often crystallinity, permanent porosity and chemical stability suffer.[39] This makes detailed studies of their efficiency with respect to targeted recognition challenging. Yaghi et al. attached macrocyclic polyethers to the linkers of MOF-1001 in order to stereospecifically accommodate paraquat dications via ion-dipole interactions.[40] More recently, Li et al. integrated the nucleobase adenine as a co-ligand into a ZnBTC-MOF and established complementary double hydrogen bonding to thymine.[41]

Here we present the successful incorporation of pyridine substituted urea groups (URPy) pending at the organic linkers of MIL-101 by postsynthetic modification without affecting the long-range order of the framework. The URPy units provide a donor-donor-acceptor sequence (DDA) as recognition pattern, which is also effective in nature[42,43] and obeys the key-and-lock principle.[36,37] We consider MIL-101 (Fig. S1) as an appropriate model framework due to its high chemical stability, large surface areas and pores in the lower mesoporous regime.[44,45] The pore dimensions meet the requirement for accommodating space demanding anchor groups and guest molecules at the same time.

We studied the sorption properties of the URPy units by using the structural isomers 2-aminopyridine (2-AP) and 3-aminopyridine (3-AP) as probe molecules. Out of these two only 2-AP presents a counterpart to the recognition pattern of the URPy units. To be able to separate the adsorption at the pending groups from the one at the CUS, the latter were also grafted with diethyl amine (DEA).[28,46] All samples were then characterized by combining multinuclear solid-state NMR spectroscopic measurements and DFT chemical shift calculations to derive structural models of preferred host-guest arrangements.

Experimental

Synthetic procedures

Al- and Cr-MIL-101-NH_2 were synthesized according to a slightly modified procedure of Hartmann et al.[47] which we previously described in ref. 48 using $AlCl_3 \cdot 6\ H_2O$ and $CrCl_3$ as metal sources.[49]

The synthesis of the ^{15}N enriched amino-terephthalic acid was performed according to the protocol of Morris et al..[50] Diethyl nitro terephthalate was synthesized from reaction of potassium nitrate (^{15}N) with diethyl terephthalate. Afterwards, diethyl amino terephthalate was obtained by treating diethyl nitro terephthalate with hydrogen (5 bar) for 24 h on a Pd/charcoal. Finally, amino terephthalic acid was obtained by reaction of diethyl amino terephthalate (^{15}N) with sodium hydroxide in a methanol/water solution.

Cr- and Al-MIL-101-URPy was obtained as follows. Referring to a synthesis route from Holt *et al.*,[51] triethylamine (1.38 mL, VWR) was added to a solution of 2-picolinic acid (1.23 g, Sigma Aldrich) in dimethylformamide (15 mL, VWR) and stirred for 30 min at RT. Then, a solution of diphenyl phosphoryl azide (2.15 mL, Sigma Aldrich) in dimethylformamide (2.5 mL, VWR) was added within 10 min under stirring. Having stirred for 3 h at RT, we poured the mixture over a water/dichloromethane solution. The organic phase was washed with a saturated solution of sodium hydrogen carbonate (VWR) in water followed by two times washing with water. After removing dichloromethane under reduced pressure, white solid 2-pyridyl acyl azide (1.12 g, 76%) was obtained in high purity as proven by solution ^1H, ^{13}C NMR and ATR-IR spectroscopy (Supporting Information). 2-pyridyl acyl azide was dissolved in dichloromethane (40 mL) and poured over dried Cr- and Al-MIL-101-NH_2 (300 mg). After refluxing for three days, we cooled the suspension to RT, centrifuged and washed two times in fresh dichloromethane. The resulting solid was dried at 100 °C for 2 h.

Liquid-phase adsorption

Prior to the sorption experiments, the commercially obtained 2-aminopyridine and 3-aminopyridine (Sigma Aldrich) were purified by sublimation, dried in a desiccator and stored in argon atmosphere. Anhydrous 1,4-dioxane (Sigma Aldrich) was used to prepare the solutions for the sorption experiments. The adsorbents were dried at 90 °C for 2 h under reduced pressure to remove physisorbed species. The liquid-phase adsorption and desorption isotherms were obtained based on the batch circulation method using a piston pump (Ismatec® IP 65), where the MOFs were successively equilibrated with the solutions of increasing and decreasing concentrations, respectively. The MIL-101 derivatives (100 mg) were mixed with dried glass beads (250 mg, Ø 30 - 50 µm, Polysciences, Inc.) and packed into a glass pipette under argon atmosphere. This generated a permeable bed which prevented densification of the MIL-101 powder to guarantee a constant flow of the solutions (8 mL) through the MIL-101 derivatives with a rate of 0.5 mL min^{-1} at room temperature. The quasi-equilibrium state was monitored every 60 min and circulation was continued until the quasi-equilibrium state was reached. The uptakes q_{eq} were determined from gas chromatographic data (Agilent 69890N) by using the differences between the initial and quasi-equilibrium concentrations as shown in equation (1)

$$q_{eq} = \frac{(c_0 - c_{eq}) \cdot V}{m} \cdot \frac{M_{framework}}{s} \quad (1)$$

where c_0 is the initial concentration of the guest molecules in the solution, c_{eq} corresponds to the concentration after reaching the quasi-equilibrium state, V is the volume of solution, m is the mass of the adsorbent, $M_{framework}$ is the molar mass of the frameworks as given in Table 1 and s represents the number of strong adsorption sites. The latter amounts to five, due to two positions at the CUS and three pending groups. For the GC analyses dodecane was used as the internal standard. The selectivity coefficients α were calculated according to equation (2)

$$\alpha = \frac{q_{2-AP}}{q_{3-AP}} \cdot \frac{c_{3-AP}}{c_{2-AP}} \quad (2)$$

where $q_{2\text{-}AP}$ and $q_{3\text{-}AP}$ are the adsorbed amounts of 2-AP and 3-AP, respectively, and $c_{2\text{-}AP}$ and $c_{3\text{-}AP}$ represent the bulk equilibrium concentrations of the respective target molecules.

Methods

Powder X-ray diffraction (PXRD) experiments were carried out in Bragg-Brentano geometry on a Panalytical X'pert Pro diffractometer equipped with a X'Celerator Scientific RTMS detector using Ni filtered $Cu_{K\alpha}$ radiation (λ = 1.54187 Å, 40 kV, 40 mA). Measurements were performed in the range of 2-30° (2θ) with a step size of 0.017°. The simulated PXRD pattern was obtained by replacing Cr by Al in a published structure model of Cr-MIL-101.[52] The cell parameters of the face centered cubic cell were refined to 87.7 Å while maintaining the space group $F\,d\bar{3}m$ (No. 227).

Attenuated total reflectance IR spectra were recorded in the range 400 - 4000 cm^{-1} with a resolution of 4 cm^{-1} on a Jasco FT/IR-6100 spectrometer with a PIKEGladiATR accessory.

The samples for chemical analyses were prepared in a glove box under argon atmosphere after evacuating at 90 °C for 2 h. Carbon, hydrogen and nitrogen contents (wt%) were obtained on a Vario elementar EL III. Aluminum and chromium contents (wt%) were determined by atomic absorption spectroscopy (AAS) in extinction mode on a Varian AA100 using a N_2O/acetylene flame upon chemical digestion in a mixture of hydrochloric acid, nitric acid and sulfuric acid. EDX spectroscopy was carried out on a Joel JSM 6400 scanning electron microscope equipped with a Noran energy dispersive X-ray analyzer and using a beam voltage of 20 kV.

Solution ^1H and ^{13}C NMR spectra were obtained using a Bruker DRX 500 spectrometer operating at a proton frequency of 500.13 MHz. Chemical shifts are given in parts per million using the DMSO-d6 peak as an internal standard according to literature values (2.54 ppm for ^1H and 40.45 ppm for ^{13}C).[53]

All solid-state NMR spectra were acquired under magic-angle spinning using ZrO_2 rotors. The chemical shifts were referenced to TMS for ^{13}C, to nitromethane for ^{15}N and to an aqueous solution of $AlCl_3 \cdot 6\,H_2O$ for ^{27}Al. ^{13}C CP MAS measurements were collected on a Bruker Avance III HD spectrometer at 9.4 T using a 4 mm double resonance probe at a spinning frequency of 10 kHz. ^{15}N CP MAS spectra were recorded on a Bruker Avance II 300 spectrometer at a spinning rate of 5 kHz using a 7 mm triple resonance probe. ^{13}C CP MAS and ^{15}N CP MAS spectra were obtained after 90° pulse excitation of 3.0 µs and 3.5 µs on the ^1H channel, respectively, and 6 µs for directly excited ^{15}N. The recycle delays for ^{13}C CP and ^{15}N CP of the frameworks were 2 s, 1800 s for ^{15}N CP of the crystalline guest molecules and 3600 s for the single pulse ^{15}N NMR measurement. The CP mixing times were set to 5 ms for ^1H-^{13}C and ^1H-^{15}N each. Broadband proton decoupling was achieved by applying the SPINAL64[54] sequence with of nutation frequency of around 80 kHz. The signal assignments of the NMR spectra were based upon simulation of the chemical shifts using the ACD/Labs software package;[55] the IR vibration bands were identified according to literature data.[48,49]

Nitrogen sorption measurements were performed on a Quantachrome NOVA 2000e at 77 K after evacuating the adsorbents at 393 K for 14 h under reduced pressure. Brunauer-Emmet-Teller (BET) equivalent surface areas were determined in the relative pressure range between 0.06 and 0.15 to accommodate for microporous materials.[56] Specific total pore volumes were determined at a relative pressure of 0.98 according to the Gurvich rule.[57] The pore-size distributions were derived using the argon NLDFT model at 77 K for the adsorption branch assuming a silica/zeolite surface and a spherical/cylindrical pore shape which is implemented in the Quantachrome ASiQ v3.0 software package.

Results and discussion

Synthesis and characterisation

Al- and Cr-MIL-101-NH_2 were prepared as previously reported.[48,49] Al- and Cr-MIL-101-URPy were synthesized after suspending Al- and Cr-MIL-101-NH_2 in a solution of 2-pyridyl acyl azide and subsequent *Curtius* rearrangement to the reactive 2-pyridyl isocyanate (Scheme 1). Attempts to isolate and then use 2-pyridyl isocyanate for the PSM reaction failed because of dimerization of the reactive isocyanates.[51] Therefore, we isolated 2-pyridyl acyl azide after synthesis from 2-picolinic acid (Figs. S2-S4, ESI) and loaded the azide species over the internal surface of MIL-101-NH_2. Thus, the spatially separated 2-pyridyl isocyanate reacts more likely with the closer amino groups than to undergo a dimerization (black bend arrow within Scheme 1).

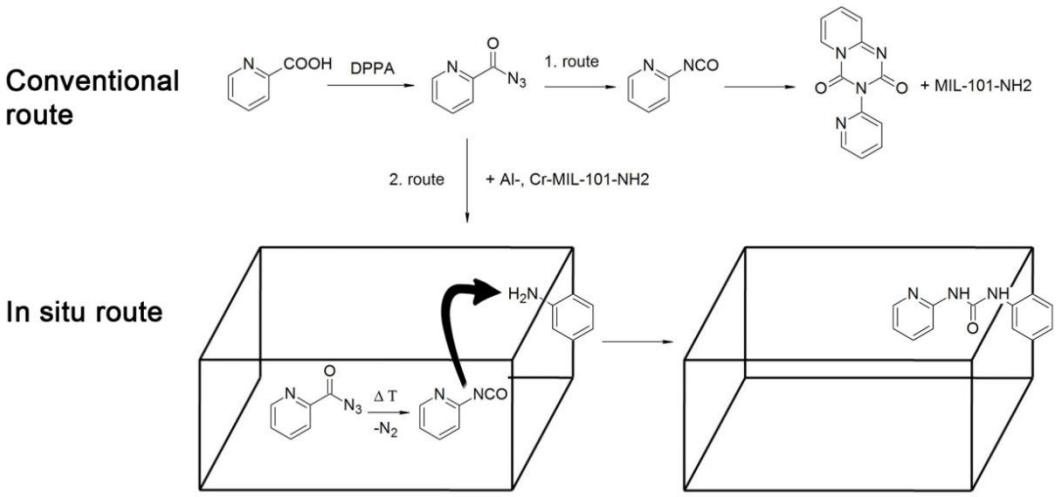

Scheme 1 Conventional and *in situ* routes for the synthesis of Al/Cr-MIL-101-URPy. Both routes are based on the preparation of 2-pyridyl acyl azide. While conventionally the *Curtius* rearrangement to 2-pyridyl isocyanate is carried separately, 2-pyridyl isocyanate is created in situ within the pore space of MIL-101-NH_2 (represented by the scaffold) after loading the frameworks with 2-pyridyl acyl azide.

View Article Online
DOI: 10.1039/C8TA12190G

Journal Name

ARTICLE

The inorganic building units of Cr-MIL-101-NH_2 and Cr-MIL-101-URPy were grafted with diethylamine (DEA) following the protocol of Hwang et al.[46] The activation of the accessible terminal metal sites (CUS) was carried out at 120 °C for all frameworks to avoid degradation of the URPy pending group at higher temperatures.

The PXRD patterns of all products fully coincide with those of the respective parent MOFs and the simulated powder patterns. This confirms successful MOF syntheses and retention of the structure after PSM without formation of crystalline side products (Fig. S5). The slight intensity variations are attributed to disorder of the pending pyridyl urea and diethyl amine groups.

The PSM of the organic linkers was monitored by ^{13}C and ^{15}N NMR spectroscopy of the diamagnetic Al-MIL-101 derivatives. The most characteristic changes within the ^{13}C MAS NMR spectra were observed for the signal of the amino bearing carbon at 151.5 ppm (Fig. 1a, black line), which shifts to 137.4 ppm upon PSM accompanied by the emergence of a signal for the urea carbon at 152.1 ppm (Fig. 1a, red line). Upon PSM the ^{15}N NMR amino signal of Al-MIL-101-NH_2 at -316 ppm vanishes (Fig. 1b, black line), whereas the ones for the pyridyl urea group appear at -272.7 ppm, -263.7 ppm and -96.5 ppm (Fig. 1b, red line). Together with intensity changes for the characteristic vibrational bands of the amino and pyridyl urea groups within the IR spectra (Fig. S8), we expect an almost quantitative PSM for the Al- and Cr-MIL-101 derivatives.

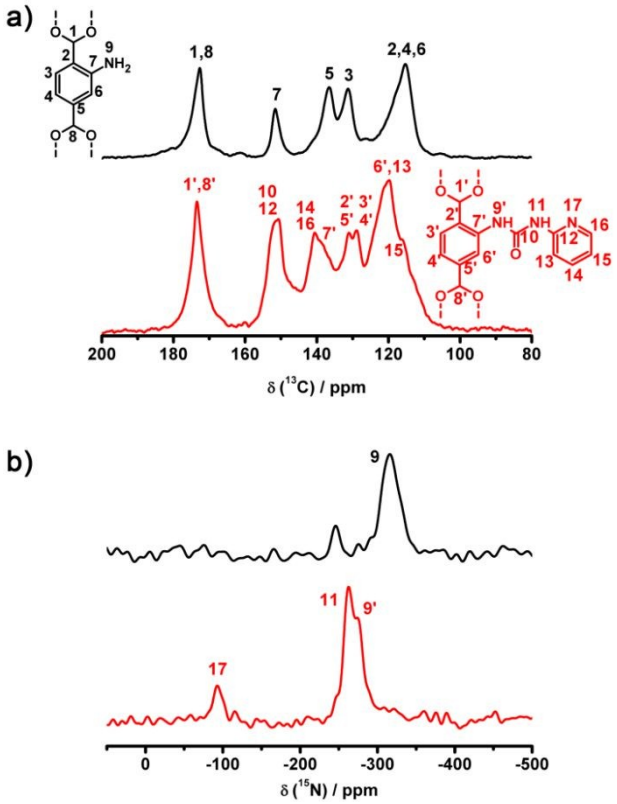

Fig. 1 a) ^{13}C CP MAS NMR spectra of Al-MIL-101-NH_2 (black line) and Al-MIL-101-URPy (red line) and b) ^{15}N CP MAS NMR spectra of Al-MIL-101-NH_2 (black line) and Al-MIL-101-URPy (red line) including assignment of all resonances. The weak signal at -247 ppm within the ^{15}N MAS spectrum of Al-MIL-101-NH_2 (black line) was attributed to a formamide moiety, which might form by a side reaction of DMF and the amino groups. Its total amount is less than 5%. For more information refer to Fig. S6.

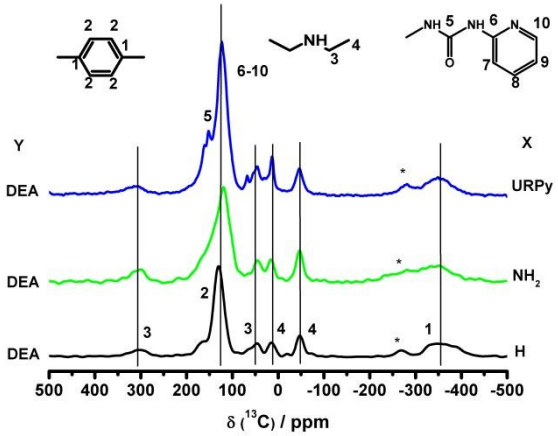

Fig. 2 ^{13}C MAS NMR spectra of DEA-Cr-MIL-101-H (black line), DEA-Cr-MIL-101-NH_2 (green line) and DEA-Cr-MIL-101-URPy (blue line).

For the Cr-MIL-101 derivatives grafted with DEA, the ^{13}C pNMR spectra (Fig. 2) exhibit both hyperfine shifted and diamagnetic resonances. This is typical for DEA coordinated to the CUS of the IBU (hyperfine shifted signals) and DEA physisorbed in a second coordination sphere (diamagnetic shifts).[28] For the DEA@MIL-101-URPy, we observed additional resonances between 140 and 160 ppm, originating from the URPy groups. The incorporation of DEA is also supported by the small blueshifts of 9 cm^{-1} and 7 cm^{-1} for the aliphatic methylene C-H and C-N stretching vibration bands of coordinated DEA and free ligand (Fig. S8b). These shifts are in line with the results for other alkyl amines adsorbed at metal centres.[46,58,59]

Based on these results, EDX, AAS, elemental analysis and ^1H solution NMR spectroscopy (after digesting the products in basic solutions) allowed to determine the chemical composition of the frameworks and the yields of grafting with DEA as well as of the PSM (URPy). Details of the corresponding analyses are given in the supporting information (Figs. S9 and S10 and Table S1). The resulting formula units are summarized in Table 1. In total, the PSM of the amino into the pyridine urea pending groups was achieved with a yield of about 90% for both the chromium and aluminum frameworks. For the exchange of water with DEA molecules at the CUS of the Cr-MIL-101-X derivatives a conversion degree larger than 60% was reached.

View Article Online
DOI: 10.1039/C8TA12190G

Table 1 Experimental formula units for the synthesized MIL-101 derivatives.

	Formula unit
Al-MIL-101-NH_2	$Al_3O(H_2O)_2Cl(bdc)_3$
Al-MIL-101-URPy	$Al_3O(H_2O)_2Cl(bdc\text{-}NH_2)_{0.3}(bdc\text{-}URPy)_{2.7}$
H_2O-Cr-MIL-101-NH_2	$Cr_3O(H_2O)_{2.1}Cl_{0.9}(bdc\text{-}NH_2)_3$
DEA-Cr-MIL-101-NH_2	$Cr_3O(H_2O)_{0.85}(DEA)_{1.5}Cl_{0.95}(bdc\text{-}NH_2)_3$
H_2O-Cr-MIL-101-URPy	$Cr_3O(H_2O)_{2.04}Cl_{0.96}(bdc\text{-}NH_2)_{0.3}(bdc\text{-}URPy)_{2.7}$
DEA-Cr-MIL-101-URPy	$Cr_3O(H_2O)_{1.05}(DEA)_{1.2}Cl_{0.97}(bdc\text{-}NH_2)_{0.3}(bdc\text{-}URPy)_{2.7}$

Nitrogen sorption isotherms reveal lower porosities after PSM for Al-MIL-101-NH_2 and Cr-MIL-101-NH_2 (Fig. S11 a,c). The bulkier URPy groups reduced the apparent BET surface areas and total pore volumes by nearly 50 % from 2340 $m^2\ g^{-1}$ and 1650 $m^2\ g^{-1}$ for Al-MIL-101-NH_2 and Cr-MIL-101-NH_2 to 1325 $m^2\ g^{-1}$ and to 779 $m^2\ g^{-1}$ for the URPy derivatives (Table S2). The DEA molecules reduced the latter quantities again by about 30 % for Cr-MIL-101-NH_2 and about 20 % for Cr-MIL-101-URPy (Table S2). This is in line with the pore size distribution analyses. While for the amino derivatives cavity sizes of 2.5 nm and 3.0 nm were obtained, the URPy functionalization reduced the pores to 2.0 nm and 2.7 nm. Grafting the CUS of Cr-MIL-101-X with DEA both pores are reduced in size again by about 0.3 to 0.4 nm (Table S2 and Fig. S11 b, d).

Sorption experiments

To characterize the binding preferences and sorption properties of the pending pyridyl urea groups, which could not be incorporated into the pore space of MOFs before, we determined adsorption isotherms for H_2O@Al-MIL-101-X, H_2O@Cr-MIL-101-X and DEA@Cr-MIL-101-X with X equal to amino and pyridyl urea groups. As probe molecules, 2-AP and 3-AP were used in single and competitive experiments. For H_2O@Al-MIL-101-X additionally, desorption isotherms were collected. The sorption isotherms are depicted in Figs. 3 and S12 - S14 and are expressed as adsorbed molecules per binding formula unit (FU) as function of the equilibrium concentration of the bulk liquid phase. The calculation of the molecular weight per formula unit is based on the chemical compositions of the frameworks (Table 1).

The single adsorption isotherms (Fig. S12) show almost identical uptakes for the pairs H_2O@Al-MIL-101-NH_2 / H_2O@Cr-MIL-101-NH_2 and H_2O@Al-MIL-101-URPy / H_2O@Cr-MIL-101-URPy. This was observed for 2-AP and 3-AP, respectively. Furthermore, some of the desorption branches depicted in Fig. S13 show a hysteresis, which indicates that some guest molecules, probably the ones attached to the CUSs at the IBU, are harder to remove than the ones interacting with the side chains. For the Cr-MIL-101 framework it is known, that both probe molecules interact strongly with the CUS at the IBUs.[28] Due to the equivalence of the single adsorption isotherms for the above-mentioned pairs we expect a similar behavior for the Al-MIL-101 derivatives. Indeed, the ^{27}Al MAS NMR spectra of 2-AP@Al-MIL-101-NH_2 and 3-AP@Al-MIL-101-NH_2 show a significantly more asymmetric line shape compared to H_2O@Al-MIL-101-NH_2 (Fig. S15). We attribute this to a larger second-order quadrupolar interaction, due to an increasingly asymmetric charge distribution after attaching 2-AP and 3-AP, respectively.

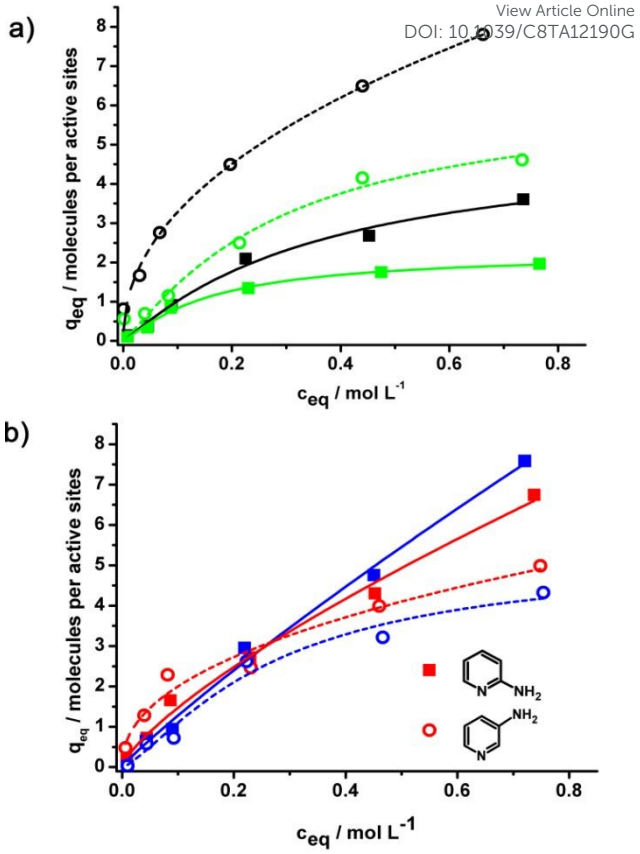

Fig. 3 Competitive adsorption isotherms of 2-AP (solid squares) and 3-AP (empty circles) on a) Al-MIL-101-NH_2 (black curves) and DEA-Cr-MIL-101-NH_2 (green curves); b) Al-MIL-101-URPy (red curves) and DEA-Cr-MIL-101-URPy (blue curves).

By grafting the CUS with DEA prior to the adsorption experiments, we strive to minimize the influence of the CUS on the isotherm to single out the selective adsorption at the pending groups X. Since Al-MIL-101 does not withstand the grafting conditions, these experiments were carried out for the Cr-MIL-101-X derivatives only. The reduced uptake for both 2-AP and 3-AP for the single isotherms of DEA@Cr-MIL-101-X (Fig. S12) shows, that the blocking of the CUS is effective. As such, we take differences in the competitive adsorption isotherms (mixtures of 2-AP and 3-AP) of H_2O@Al-MIL-101-X and DEA@Cr-MIL-101-X and X being amino (Fig. 3a) and pyridyl urea (Fig. 3b) groups as a measure for the selective adsorption at the pending groups.

The competitive adsorption isotherms follow Langmuir type isotherms (Fig. 3). The amino bearing derivatives (Fig. 3a) take up significantly more 3-AP from the mixture compared to 2-AP. For the highest uptakes this amounts to a factor of two and four for H_2O@Al-MIL-101-NH_2 and DEA@Cr-MIL-101-NH_2, respectively. While the uptake of 2-AP is only slightly reduced for both frameworks, blocking the CUS reduces the uptake of 3-AP by 50%. This follows the binding affinity derived before[28] and demonstrates that 3-AP is preferentially attached to the CUS, while 2-AP is adsorbed in an unspecific fashion. For the pyridyl urea derivatives the uptake of 2-AP is strongly enhanced. Compared to the amino MIL-101 this results in a factor of five. Simultaneously, the uptake of 3-AP is slightly reduced compared to the amino derivatives. Grafting the CUS is apparently less effective

View Article Online
DOI: 10.1039/C8TA12190G

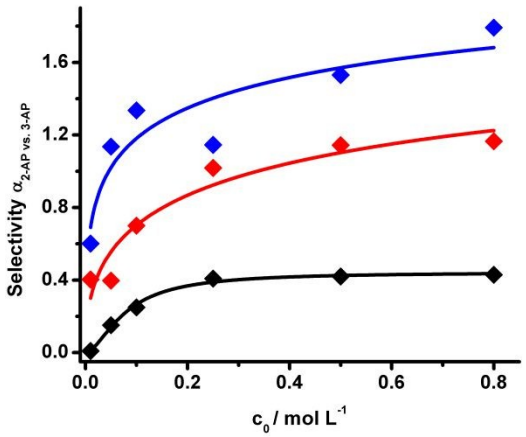

Fig. 4 Selectivity values α on Al-MIL-101-NH_2 (black curve), Al-MIL-101-URPy (red curve) and DEA-Cr-MIL-101-URPy (blue curve).

as the uptake of DEA@Cr-MIL-101-URPy is only slightly lower than the one of H_2O@Al-MIL-101-URPy. This trend is explained by two effects. On the one hand, the grafting reaction is less efficient for the pyridyl urea derivatives leaving roughly 40% of the CUS accessible. On the other hand, the interactions of 3-AP and 2-AP with the pyridyl urea units will be stronger, providing a stronger competition to the CUS. This effect is also observed for the ^{27}Al MAS NMR spectra of 2-AP@Al-MIL-101-URPy and 3-AP@Al-MIL-101-URPy, which are both similar to the one of H_2O@Al-MIL-101-URPy indicating that coordination to the CUS is less relevant. For 2-AP the affinity to the pending groups seems to be significantly more pronounced as shown in the increasing uptake and the expected better match with the DDA recognition pattern.

As a consequence, we observe a clear trend for the selectivity of 2-AP over 3-AP (Fig. 4) represented in the selectivity coefficient $\alpha_{2\text{-AP vs. }3\text{-AP}}$ (equation 2). While amino functionalized derivatives with active CUS exhibit a selectivity of about 0.4 at higher uptakes (Fig. 4 black curve), introducing the pyridyl urea groups increases the selectivity by roughly a factor of three. By additionally blocking the CUS, the selectivity raises again by roughly 50 %. In total, the selectivities of the amino and pyridyl urea groups differ by a factor of ≈ 4, demonstrating that the difference for the bonding affinity between a single donor (NH_2) and a donor-acceptor pattern (URPy) is large enough to separate 2-AP and 3-AP in solutions. Both PXRD data (Fig. S16) and TEM images (Figs. S17 – S18) demonstrate that neither the crystallinity nor the morphology of Al/Cr-MIL-101-X changed significantly upon loading with 2-AP, 3-AP and mixtures thereof. As such, the increase of the selectivity is attributed to the host-guest interactions.

Host guest interactions

In order to develop a better understanding for preferred binding sites at the amino and pyridyl urea groups we collected ^{15}N MAS spectra for all Al-MIL-101 derivatives as function of loading with 2-AP/3-AP. These data were compared to results of quantum chemical calculations on DFT level providing energetically favored spatial arrangements for the adducts of guests and pending groups as well as simulated isotropic chemical shifts for the nitrogen sites within these adducts. The corresponding ^{15}N MAS NMR spectra are

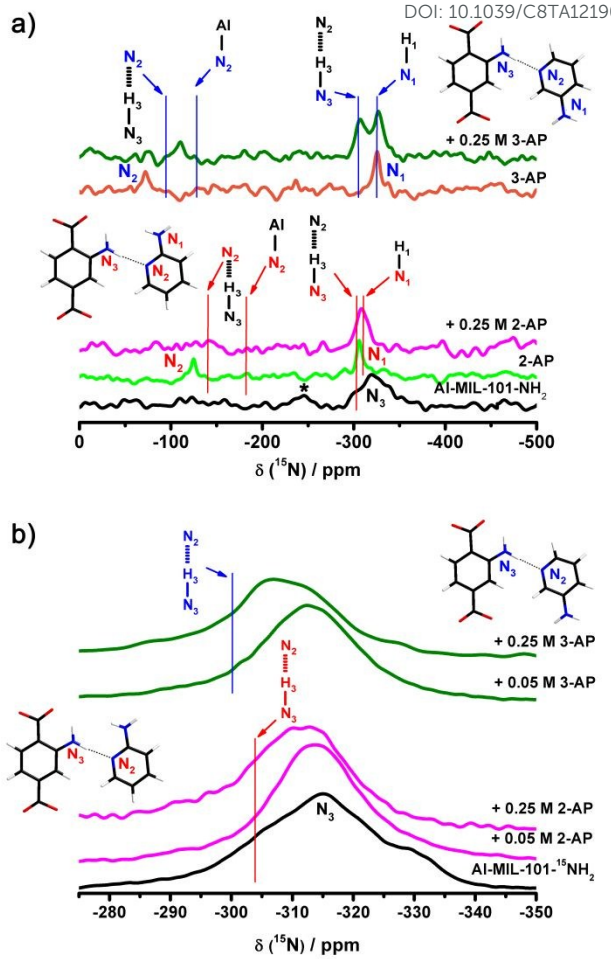

Fig. 5: a) ^{15}N NMR CP MAS spectra from top to bottom: 0.25 M 3-AP@Al-MIL-101-NH_2, 3-AP, 0.25 M 2-AP@Al-MIL-101-NH_2, 2-AP and Al-MIL-101-NH_2; b) Enlarged section of the ^{15}N NMR (98% ^{15}N labeled) spectra from top to bottom: 0.25 M 3-AP@Al-MIL-101-$^{15}NH_2$, 0.05 M 3-AP@Al-MIL-101-$^{15}NH_2$, 0.25 M 2-AP@Al-MIL-101-$^{15}NH_2$, 0.05 M 2-AP@Al-MIL-101-$^{15}NH_2$ and Al-MIL-101-$^{15}NH_2$. The vertical lines in a) and b) represent calculated δ_{iso} values for the model with the best match to the experimental data. The corresponding structure is depicted on the left (3-AP) and right (2-AP). The asterisk denotes a small impurity of NHCHO units (Fig. S6).

depicted in Figs. 5 – 7 and the simulated δ_{iso} values for the most likely adducts are plotted in colored vertical lines.

The spectrum of 3-AP@Al-MIL-101-NH_2 shows three signals at -109 ppm (**N_2**), -303 pm (**N_3**) and -325 ppm (**N_1**) (Fig. 5a, olive line). They match 3-AP@amino adducts best, where the pyridine nitrogen (N_2) of 3-AP is hydrogen bonded to one of the amino protons (**N_3-H_3**). This causes a downfield shift for **N_3** and an upfield shift for **N_2** compared to pure 3-AP and H_2O@MIL-101-NH_2 (Fig. 5a, orange and black lines). The signal for the amino groups of 3-AP (**N_1**), which do not participate to the adduct formation, is not affected. In spite of the broadening of the resonances within the ^{27}Al MAS spectra of 2-AP/3-AP@MIL-101-NH_2 (Fig. S15), which hints towards a competing interaction of the guest molecules with the CUS, no resonances for the corresponding adducts could be singled out within the ^{15}N MAS NMR spectra (Fig. 5a). Characteristic resonances for adducts should cause upfield shifts for the pyridine nitrogen (**N_2**) by approximately

40-50 ppm according to DFT calculations and literature data.[60] We thus conclude that at RT the equilibrium between adsorption at the CUS and the pending groups is dynamic with exchange rates in the fast motion regime. Thus, only one averaged resonance at -109 ppm (**N_2**, 3-AP) is visible within the ^{15}N MAS NMR spectra.

A similar trend is observed for the ^{15}N MAS NMR spectrum (Fig. 5a, magenta line) of 2-AP@Al-MIL-101-NH_2, which exhibits resonances at about -142 ppm (**N_2**) and -306 ppm (**N_3-H_3**, **N_1**). The heavy overlap of the signals for **N_3** and **N_1**, however, does not allow to determine the downfield shift quantitatively and thus prevents to judge the binding preference of 2-AP and 3-AP at the amino function of the framework. The resonance assigned to **N_2** matches closely the simulated δ_{iso} for the fragment 2-AP@bcd-NH_2, which hints to a preferential adsorption of 2-AP at the amino function. This in line with the weaker binding strength of 2-AP compared to 3-AP at the CUS.[28]

By labeling Al-MIL-101-NH_2 with ^{15}N at the amino group we could single out the characteristic resonances for the free amino units as well as for the 2-AP/3-AP@amino adducts (Fig. 5b). With increasing guest loading the downfield shift rises for both guests reaching 4.4 ppm for 2-AP and 7.5 ppm for 3-AP after equilibrating with solutions of 0.25 M for each guest. This suggests, that 3-AP exhibits a higher binding affinity to the amino function compared to 2-AP, which is in line with an energy lower by 6 kJ/mol for 3-AP as derived from the DFT calculations.

In case of Al-MIL-101-URPy the DFT calculations suggest that the urea fragment close to the linker **N_3-H_3** forms a strong hydrogen bond with the oxygen atoms of neighboring carboxylate groups of the terephthalates. Therefore, the **N_3-H_3** fragment is not available for hydrogen bonding to the guest molecules 2-AP/3-AP and reduces the DDA to a DA pattern. This is experimentally supported as the ^{15}N NMR shift of **N_3** at -273.5 ppm is essentially independent of the guest loading (Fig. 6 and 7).

The ^{15}N MAS NMR spectra of 2-AP@Al-MIL-101-URPy exhibit resonances typical for the urea pyridyl group and 2-AP molecules (Table S3). With respect to the single component phases 2-AP and Al-MIL-101-URPy the resonances for the amino group **N_1**, the outer amido fragment **N_4** and the pyridyl nitrogen **N_2** of 2-AP are downfield-shifted by roughly 9, 3 and 7 ppm. Simultaneously, the pyridyl nitrogen of the URPy unit (**N_5**) shift upfield by 5 ppm. These trends become more pronounced with higher loading and lower temperatures as the hydrogen bonds between the pending groups and the guests become stronger (Fig. 6). These findings are matched best with the prediction of isotropic chemical shifts at the DFT level (vertical lines within Fig. 6 and Table S3) for a scenario where 2-AP and the pending URPy groups form the complementary hydrogen bond pattern DA···AD. According to the DFT calculations this scenario it energetically favored by roughly 80 kJ/mol with respect to the single component phases. Additionally, for higher loadings also 2-AP adsorbed in an unspecific fashion was observed as demonstrated by the ^{15}N NMR signal at around -307.0 ppm, which is typical for 2-AP in its crystalline form (Fig. 6, green line).

In contrast, the DFT calculations suggested at least two possible arrangements for 3-AP within Al-MIL-101-URPy. Both are depicted in Fig. 7. For the first one, 3-AP forms weak H- bonds between its pyridine nitrogen **N_2** and the **N_4-H_4** unit of the urea fragment and between the aromatic C-H bond in ortho position to **N_2** and the pyridine nitrogen atom **N_5** of URPy. This induces significant high- and lowfield shifts for the resonances of **N_2** and **N_4**, while the one for **N_5** remains essentially unchanged. The second scenario is stabilized by a single H bond between the amino hydrogen atom **N_1-H_1** of 3-AP and the pyridine nitrogen **N_5** of the pending urea pyridyl groups. Again, the resonance for the amino function (**N_1**) is shifted downfield while the signal for **N_5** shifts highfield. While the double H-bond scenario is favored by 50 kJ/mol with respect to the single component phases according to the DFT calculations the single H-bond scenario is

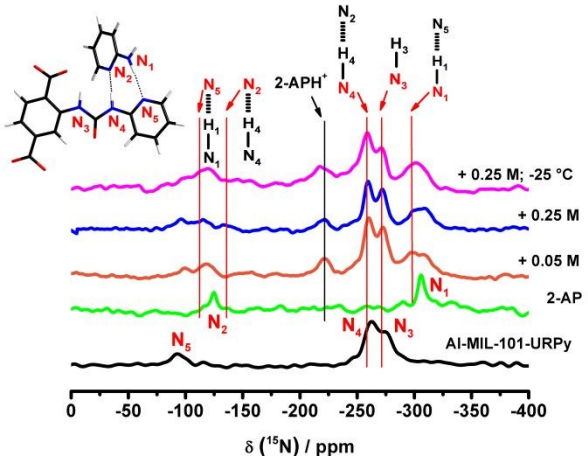

Fig. 6 ^{15}N CP MAS NMR spectra of Al-MIL-101-URPy (black line), 2-AP (green line), 0.05 M 2-AP@Al-MIL-101-URPy (orange line), 0.25 M 2-AP@Al-MIL-101-URPy (blue line) and 0.25 M 2-AP@Al-MIL-101-URPy at -25 °C (magenta line). Red vertical lines represent the chemical shifts derived from preferred arrangements of 2-AP within Al-MIL-101-URPy. The black vertical line corresponds to the chemical shift of **N_2** for protonated 2-AP (2-APH$^+$).[61]

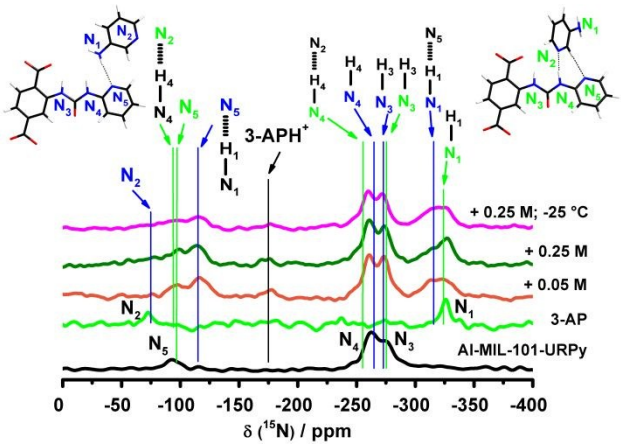

Fig. 7 ^{15}N CP MAS NMR spectra of Al-MIL-101-URPy (black line), 3-AP (green line), 0.05 M 3-AP@Al-MIL-101-URPy (orange line), 0.25 M 3-AP@Al-MIL-101-URPy (olive line) and 0.25 M 3-AP@Al-MIL-101-URPy at -25 °C (magenta line). The green and blue vertical lines indicate the chemical shifts derived from most preferred arrangements. The black vertical line corresponds to the chemical shift of N_2 for protonated 3-AP (3-APH$^+$).[61]

stabilized by roughly 30 kJ/mol. The respective ^{15}N chemical shifts are given in Table S3.

The observed ^{15}N NMR spectra of 3-AP@Al-MIL-101-URPy exhibit resonances typical for of both arrangements (Fig. 7 and Table S3) for all loadings and temperatures. In spite of the stronger stabilization for the double H-bond scenario no clear trend for the intensities assigned to both scenarios is visible. This indicates that both scenarios exhibit similar interaction strengths experimentally. We attribute this to secondary interactions with further guest and solvent molecules which might lead to additional stabilizing contributions. The latter could not be considered for the DFT calculations.

Both the ^{15}N NMR spectra for 2-AP@Al-MIL-101-URPy (Fig. 6) and 3-AP@Al-MIL-101-URPy (Fig. 7) exhibit an additional resonance at -220 ppm (2-AP@Al-MIL-101-URPy) and –176 ppm (3-AP@Al-MIL-101-URPy). Both signals are typical, for guest molecules protonated at the pyridyl nitrogen atoms.[61] We attribute this to an increased acidity of residual water in the vicinity of the pending URPy groups, which partially protonate the guest molecules.

Conclusions

Here we report on the successful incorporation of a 2-pyridyl urea side group with an apparent DDA hydrogen bond donor-acceptor pattern into the framework topology MIL-101 with pore cavities in the mesoporous range. For this, the parent material MIL-101-NH_2 was modified postsynthetically by loading it with 2-pyridyl acyl azide solutions. The reactive intermediate 2-pyridyl isocyanate, formed *in situ* in the pore space, then reacts preferentially with the amino functions of the framework to the desired product with a yield of about 90 % instead of undergoing a dimerisation.

The influence of the pending URPy groups on the sorption properties of MIL-101-URPy was studied by using a combination of solution phase sorption experiments, multinuclear MAS NMR spectroscopy and DFT calculations for various model systems. All energetically favored structure models feature a strong intra framework hydrogen bond between the inner urea N-H units and the adjacent carboxylate groups of the terephthalate linkers. We thus expect the pyridyl urea groups to act as a double hydrogen bond donor-acceptor (DA) within the framework instead of the DDA pattern typical for free URPy groups. As probe molecules for the sorption preferences, we thus loaded MIL-101-URPy frameworks with organic solutions of 2-AP and 3-AP. While 2-AP matches both function and geometry of the accessible hydrogen bond donor-acceptor sequence of the pending URPy groups, 3-AP does not.

By analyzing the response of two pairs of MIL-101 derivatives – Al-MIL-101-NH_2 and Cr-MIL-101-NH_2 as well as Al-MIL-101-URPy and Cr-MIL-101-URPy on single component and competitive adsorption isotherms, we were able to separate the influence of the pending URPy groups from CUSs at the metal centers of the IBUs. While the higher chemical stability of Cr-MIL-101-X enabled us to block the CUS with diethyl amine and thus to reduce their influence on the adsorption isotherms markedly, the diamagnetic Al-MIL-101-X derivatives lead to well resolved ^{15}N MAS NMR spectra. We then compared the observed chemical shifts with the ones calculated for the DFT model systems to probe preferred adsorption sites at the side groups.

Both H_2O@Al-MIL-101-NH_2 and H_2O@Cr-MIL-101-NH_2 showed enhanced uptakes and selectivities for 3-AP. By blocking the CUS with DEA the uptake for both 2-Ap and 3-AP is reduced with a stronger effect for 3-AP. This suggests, that 3-AP exhibits a higher affinity to the CUS compared to 2-AP. At the same time, both guest molecules are attached to the pending amino functions by single hydrogen bonds between the pyridine nitrogen and the NH unit of the amino functions as indicated by the ^{15}N MAS NMR spectra as function of the guest loading.

After introducing the pending URPy groups the selectivity for 2-AP is enhanced by a factor of three and blocking the CUS for DEA@Cr-MIL-101-URPy increases the selectivity by another 50%. The latter effect is mainly caused by a reduction of the uptake of 3-AP. The ^{15}N MAS NMR spectra collected for 2-AP/3-AP@Al-MIL-101-URPy demonstrated that 2-AP is indeed adsorbed at the pending URPy groups according to the key-and-lock principle via complementary double hydrogen bonds, while for 3-AP two scenarios seem to be equally attractive. Both of these arrangements feature one single hydrogen bond only and are thus less favored by roughly 30 kJ/mol compared to the double hydrogen bond scenario realized with 2-AP.

Our results suggest that introducing selectivity into the sorption processes of MOFs can be established by introducing side groups with multiple hydrogen bonding motifs, which are selected to bind targeted guest molecules via the key-and-lock principle of supramolecular chemistry. The concept is realized straightforwardly and can thus be applied not only to MOFs but to a broad variety of porous materials. This offers potential for targeted recognition of larger and complex molecules, which is necessary for applications like specific separation, sensors and drug delivery.

Conflicts of interest

There are no conflicts of interest to declare.

Acknowledgements

We gratefully acknowledge financial support by the DFG (SE 1417/7-1 and SE 1417/8-1 as well as LO 1801/4-1 within the SPP1928). We thank Beate Bojer for her steady support with the NMR measurements.

Notes and references

1 J.-R. Li, R. J. Kuppler and H.-C. Zhou, *Chem. Soc. Rev.*, 2009, **38**, 1477–1504.

2 J. Li, J. Sculley and H. Zhou, *Chem. Rev.*, 2012, **112**, 869–932.

3 K. Sumida, D. L. Rogow, J. A. Mason, T. M. Mcdonald, E. D. Bloch, Z. R. Herm, T. Bae and R. Long, *Chem. Rev.*, 2012, **112**, 724–781.

4 B. Van de Voorde, B. Bueken, J. Denayer and D. De Vos,

Chem. Soc. Rev., 2014, **43**, 5766–88.
5 A. Samokhvalov, *Chem. Eur. J.*, 2015, **21**, 16726–16742.
6 P. Horcajada, R. Gref, T. Baati, P. K. Allan, G. Maurin and P. Couvreur, *Chem. Rev.*, 2012, **111**, 1232–1268.
7 P. Horcajada, T. Chalati, C. Serre, B. Gillet, C. Sebrie, T. Baati, J. F. Eubank, D. Heurtaux, P. Clayette, C. Kreuz, J.-S. Chang, Y. K. Hwang, V. Marsaud, P.-N. Bories, L. Cynober, S. Gil, G. Férey, P. Couvreur and R. Gref, *Nat. Mater.*, 2010, **9**, 172–178.
8 A. C. McKinlay, R. E. Morris, P. Horcajada, G. Férey, R. Gref, P. Couvreur and C. Serre, *Angew. Chemie Int. Ed.*, 2010, **49**, 6260–6266.
9 A. D. Burrows, *Chem. Soc. Rev.*, 2015, **44**, 4290–4321.
10 L. E. Kreno, K. Leong, O. K. Farha, M. Allendorf, R. P. Van Duyne and J. T. Hupp, *Chem. Rev.*, 2012, **112**, 1105–1125.
11 M. L. Foo, R. Matsuda and S. Kitagawa, *Chem. Mater.*, 2014, **26**, 310–322.
12 H. Furukawa, K. E. Cordova, M. O'Keeffe and O. M. Yaghi, *Science*, 2010, **9**, 1230444.
13 A. G. Slater and A. I. Cooper, *Science*, 2015, **348**, aaa8075-1-aaa8075-10.
14 Z. Wang and S. M. Cohen, *Chem. Soc. Rev.*, 2009, **38**, 1315–1329.
15 T. Ahnfeldt, D. Gunzelmann, J. Wack, J. Senker and N. Stock, *CrystEngComm*, 2012, **14**, 4126–4136.
16 M. Lammert, S. Bernt, F. Vermoortele, D. E. De Vos and N. Stock, *Inorg.Chem.*, 2013, **52**, 8521–8528.
17 K. K. Tanabe and S. M. Cohen, *Chem. Soc. Rev.*, 2011, **40**, 498–519.
18 K. K. Tanabe, Z. Wang and S. M. Cohen, *J. Am. Chem. Soc.*, 2008, **130**, 8508–8517.
19 J. Wack, T. Ahnfeldt, N. Stock and J. Senker, *J. Phys. Chem. C*, 2013, **117**, 11991–20001.
20 L. Alaerts, M. Maes, L. Giebeler, P. A. Jacobs, J. A. Martens, J. F. M. Denayer, C. E. A. Kirschhock and D. E. De Vos, *J. Am. Chem. Soc.*, 2008, **130**, 14170–14178.
21 R. El Osta, A. Carlin-sinclair, N. Guillou, R. I. Walton, F. Vermoortele, M. Maes, D. De Vos and F. Millange, *Chem. Mater.*, 2012, **24**, 2781–2791.
22 L. Alaerts, C. E. A. Kirschhock, M. Maes, M. A. van der Veen, V. Finsy, A. Depla, J. A. Martens, G. V. Baron, P. A. Jacobs, J. F. M. Denayer and D. E. De Vos, *Angew. Chemie Int. Ed.*, 2007, **46**, 4293–4297.
23 L. Alaerts, M. Maes, P. A. Jacobs, F. M. Denayer and D. E. De Vos, *Phys. Chem. Chem. Phys.*, 2008, **10**, 2979–2985.
24 J. Dai, M. L. McKee and A. Samokhvalov, *J. Porous Mater.*, 2014, **21**, 709–727.
25 M. Maes, M. Trekels, M. Boulhout, S. Schouteden, F. Vermoortele, L. Alaerts, D. Heurtaux, Y. Seo, Y. K. Hwang, J. Chang, I. Beurroies, R. Denoyel, K. Temst, A. Vantomme, P. Horcajada, C. Serre and D. E. De Vos, *Angew. Chemie*, 2011, **123**, 4296–4300.
26 Z. Wang, Z. Sun, L. Kong and G. Li, *J. Energy Chem.*, 2013, **22**, 869–875.
27 B. Van De Voorde, M. Boulhout, F. Vermoortele, P. Horcajada, D. Cunha, J. S. Lee, J. Chang, E. Gibson, M. Daturi, J. Lavalley, A. Vimont, I. Beurroies and D. E. De Vos, *J. Am. Chem. Soc.*, 2013, **135**, 9849–9856.
28 T. Wittmann, A. Mondal, C. B. L. Tschense, J. J. Wittmann, O. Klimm, R. Siegel, B. Corzilius, B. Weber, M. Kaupp and J. Senker, *J. Am. Chem. Soc.*, 2018, **140**, 2135–2144.
29 K. A. Cychosz, A. G. Wong-Foy and A. J. Matzger, *J. Am. Chem. Soc.*, 2008, **130**, 6938–6939.
30 S. Achmann, G. Hagen, M. Hämmerle, I. M. Malkowsky, C. Kiener and R. Moos, *Chem. Eng. Technol.*, 2010, **33**, 275–280.
31 J. S. Lindsey, *New J. Chem.*, 1991, 153–180.
32 M. Li, S. Ishihara, Q. Ji, M. Akada, J. P. Hill and K. Ariga, *Sci. Technol. Adv. Mater.*, 2012, **13**, 053001.
33 G. K. Such, A. P. R. Johnston and F. Caruso, *Chem. Soc. Rev.*, 2011, **40**, 19–29.
34 C. S. Zehe, J. A. Hill, N. P. Funnell, K. Kreger, K. P. van der Zwan, A. L. Goodwin, H.-W. Schmidt and J. Senker, *Angew. Chemie Int. Ed.*, 2017, **56**, 4432–4437.
35 J. B. Wittenberg and L. Isaacs, in *Supramolecular Chemistry*, John Wiley & Sons, Ltd, Chichester, UK, 2012, pp. 1–19.
36 J.-M. Lehn, *Angew. Chem. Int. Ed.*, 1990, **29**, 1304–1319.
37 C. Schmuck and W. Wienand, *Angew. Chemie - Int. Ed.*, 2001, **40**, 4363–4369.
38 W. L. Jorgensen and J. Pranata, *J. Am. Chem. Soc.*, 1990, **112**, 2008–2010.
39 M. Zhang, Z. Gu, M. Bosch, Z. Perry and H. Zhou, *Coord. Chem. Rev.*, 2015, **293–294**, 327–356.
40 Q. Li, W. Zhang, O. S. Miljanic, C. Sue, Y.-L. Zhao, L. Liu, C. B. Knobler, J. F. Stoddart and O. M. Yaghi, *Science*, 2009, **325**, 855–859.
41 H. Cai, M. Li, X. R. Lin, W. Chen, G. H. Chen, X. C. Huang and D. Li, *Angew. Chemie - Int. Ed.*, 2015, **54**, 10454–10459.
42 M. R. Jones, N. C. Seeman and C. A. Mirkin, *Science*, 2015, **347**, 1260901–1260901.
43 S. Sivakova, S. J. Rowan and S. J. Rowan, *Chem Soc Rev*, 2005, **34**, 9–21.
44 G. Férey, C. Mellot-Draznieks, C. Serre, F. Millange, J. Dutour, S. Surblé and I. Margiolaki, *Science*, 2005, **309**, 2040–2042.
45 P. Serra-Crespo, E. V Ramos-Fernandez, J. Gascon and F. Kapteijn, *Chem. Mater.*, 2011, **23**, 2565–2572.
46 Y. K. Hwang, D. Hong, J. Chang, S. H. Jhung, Y. Seo, J. Kim, A. Vimont, M. Daturi, C. Serre and G. Férey, *Angew. Chemie Int. Ed.*, 2008, **47**, 4144–4148.
47 M. Hartmann and M. Fischer, *Microporous Mesoporous Mater.*, 2012, **164**, 38–43.
48 T. Wittmann, R. Siegel, N. Reimer, W. Milius, N. Stock and J. Senker, *Chem. Eur. J.*, 2015, **21**, 314–323.
49 S. Bernt, V. Guillerm, C. Serre and N. Stock, *Chem. Commun.*, 2011, **47**, 2838–2840.
50 W. Morris, R. E. Taylor, C. Dybowski, O. M. Yaghi and M. A. Garcia-Garibay, *J. Mol. Struct.*, 2011, **1004**, 94–101.
51 J. Holt, T. Andreassen, J. M. Bakke and A. Fiksdahl, *J. Heterocycl. Chem.*, 2005, **42**, 259–264.
52 O. I. Lebedev, F. Millange, C. Serre, G. Van Tendeloo and G. Férey, *Chem. Mater.*, 2005, **17**, 6525–6527.
53 H. E. Gottlieb, V. Kotlyar and A. Nudelman, *J. Org. Chem.*, 1997, **62**, 7512–7515.

View Article Online
DOI: 10.1039/C8TA12190G

54 B. M. Fung, A. K. Khitrin and K. Ermolaev, *J. Magn. Reson.*, 2000, **142**, 97–101.
55 I. ACD/Structure Elucidator, version 15.01 , Advanced Chemistry Development, 2013.
56 M. Thommes, *Chemie Ing. Tech.*, 2010, **82**, 1059–1073.
57 L. Gurvich, *J. Russ. Phys. Chem. Soc.*, 1915, **47**, 805–827.
58 M. Wickenheisser, F. Jeremias, S. K. Henninger and C. Janiak, *Inorganica Chim. Acta*, 2013, **407**, 145–152.
59 K. Krishnan and R. A. Plane, *Inorg. Chem.*, 1966, **5**, 852–857.
60 A. Marek, R., Lycka, *Curr. Org. Chem.*, 2002, **6**, 35–66.
61 W. Städeli and W. Philipsborn, *Helv. Chim. Acta*, 1980, **63**, 504–522.

View Article Online
DOI: 10.1039/C8TA12190G

Journal Name

ARTICLE

TOC Graphics